Clays and Clay Minerals, Vol. 44, No. 5, 658–664, 1996.

THE NATURAL OCCURRENCE OF ETA-ALUMINA (η-Al_2O_3) IN BAUXITE

DAVID B. TILLEY AND RICHARD A. EGGLETON

Centre for Australian Regolith Studies, Australian National University, Canberra, ACT, 0200, Australia

Abstract—Approximately 20 wt.% of the bauxite from Andoom in northern Queensland, Australia is composed of material that cannot be accounted for by identifiable well-crystallized phases. This poorly-diffracting material (PDM), found within the core of bauxitic pisoliths, has similar characteristics to that of eta-alumina (η-Al_2O_3); a cubic form of alumina. A differential XRD pattern of the PDM displayed a series of broad diffraction maxima attributed to eta-alumina with a mean crystal size of 9 nm. Unit cell refinement, on the basis of a cubic cell, gave a lattice parameter of a = 7.98 Å for Andoom eta-alumina. TEM and selected-area electron diffraction revealed the PDM to be composed of minute (10 nm wide), randomly oriented crystals of eta-alumina in close association with Al-hematite. Chemical analysis using a nanoprobe showed Andoom eta-alumina to be almost pure alumina with <2 *M*% Fe, <1 *M*% Si and <1 *M*% Ti. The closely associated Al-hematite may contain as much as 22 *M*% Al, however a value closer to the theoretical limit of 17 *M*% is more likely. A broad absorption band at 3450 cm^{-1} and 1630 cm^{-1} in the infra-red spectrum of the PDM indicates the presence of a substantial quantity of H_2O, strongly adsorbed onto the surface of the crystals. This is presumably due to η-Al_2O_3's large surface area of approximately 2200 m^2/g. The natural occurrence of η-Al_2O_3 in bauxite may be the result of low H_2O activities within the micro-environment of pores at the time of crystallization. The epigenetic replacement of kaolinite with η-Al_2O_3 and Al-hematite is put forward as an explanation for the formation of bauxitic pisoliths at Andoom.

Key Words—Akdalaite, Bauxite, Chi-alumina, Eta-alumina, Gamma-alumina, Pisoliths, Poorly-diffracting material, Tohdite.

INTRODUCTION

Two crystalline alumina phases have recently been reported in Australian bauxites. Tilley and Eggleton (1994) reported that bauxitic pisoliths from Weipa, North Queensland contained material which yielded very broad diffraction maxima that could not be accounted for by identifiable well-crystallized minerals. Such material, termed poorly-diffracting material (PDM), was shown to be composed predominantly of tohdite ($5Al_2O_3 \cdot H_2O$). A recent letter from the International Mineralogical Association Commission on New Minerals and Mineral Names (CNMMN) discouraged the use of the name "tohdite" in any proposed publications due to it being an invalid mineral name. The name akdalaite ($4Al_2O_3 \cdot H_2O$) was approved by the CNMMN for the mineral corresponding to tohdite, due to their similarity, and as a consequence, Weipa tohdite will now be referred to as akdalaite. Singh and Gilkes (1995) reported the occurrence of poorly crystalline chi alumina (χ-Al_2O_3) in the bauxites of Darling Range, Western Australia. The authors demonstrated that χ-Al_2O_3 formed by the dehydration of an aluminous gel-like material. Examination of bauxitic pisoliths from Andoom, which is 15 km north of Weipa, has revealed the presence of another poorly-diffracting phase, distinct from akdalaite and χ-Al_2O_3. Differential XRD and transmission electron microscopy (TEM) of the PDM showed that the phase has similar characteristics to that of η-Al_2O_3. Stumpf et al. (1950) described eta-alumina as having a cubic, spinel-type structure with a lattice parameter of 7.94 Å. Selected area electron diffraction of synthetic η-Al_2O_3 by Lippens and de Boer (1964) reported it to be tetragonally deformed with c/a ranging between 0.985 and 0.993. Zhou and Snyder (1991) demonstrated that the crystal structure of η-Al_2O_3 is essentially cubic, however somewhat spinel deformed with a = 7.914 Å. Brown et al. (1953) showed that η-Al_2O_3 is a transition phase produced by the thermal decomposition of poorly crystalline boehmite (AlO(OH)) or well-crystallized bayerite (β-$Al(OH)_3$). Further heating of η-Al_2O_3 leads to the formation of theta-alumina (θ-Al_2O_3) followed by corundum (α-Al_2O_3).

EXPERIMENTAL METHODS

The core of a bauxitic pisolith from Andoom (1 to 1.5 m depth) was sampled using a dental drill. The extracted material was finely ground using a mortar and pestle and then applied to a low-background holder. An XRD pattern of the sample was obtained by scanning over a period of 12 h. A differential XRD pattern was produced by subtracting the calculated pattern for each of the well-crystallized components, in proportion to their weight fraction. The resulting differential XRD pattern was compared with minerals and inorganic compounds in the Powder Diffraction File published by the Joint Committee on Powder Diffraction Standards. When it was found that the d-spacing values of the broadest peaks in the XRD pattern matched well with those of eta-alumina, quantitative analysis of the XRD pattern was undertaken using SIROQUANT, which is a Rietveld-type quantitative-

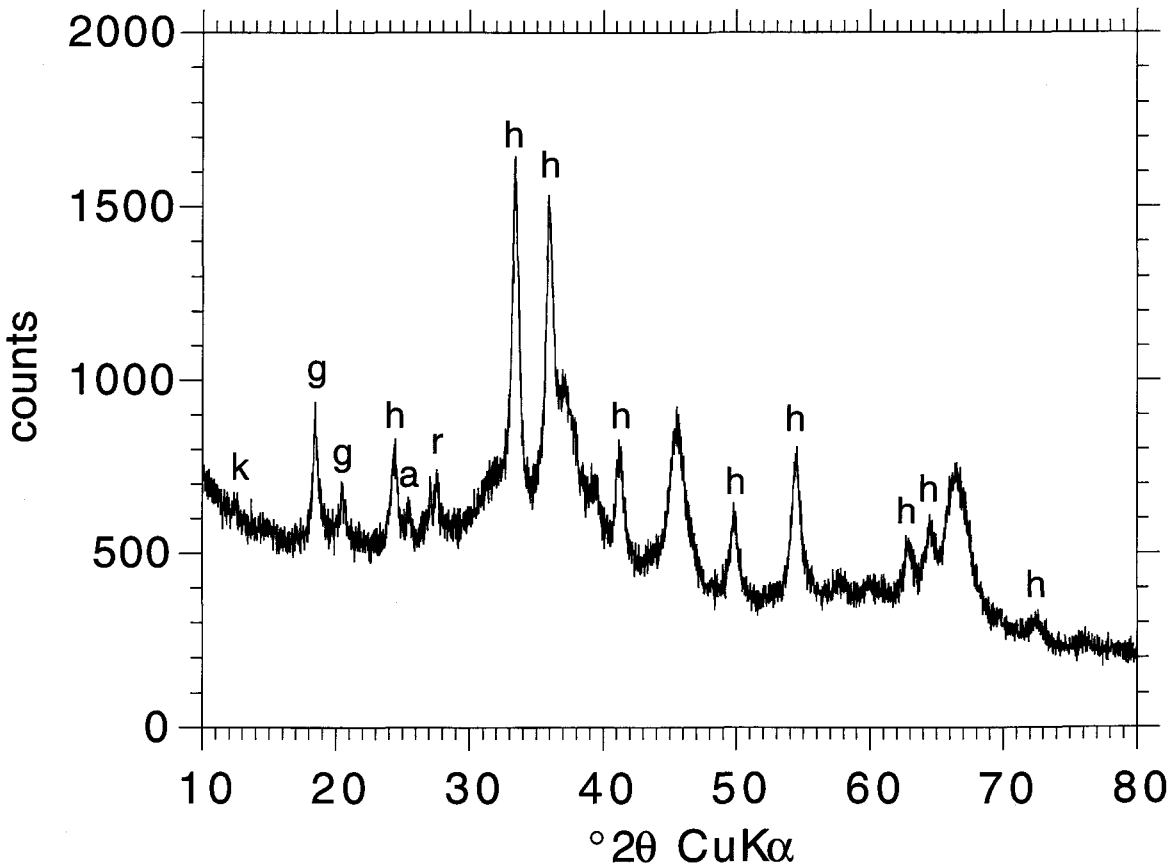

Figure 1. An XRD of PDM-rich bauxite extracted from the core of a pisolith from Andoom in northern Queensland. Key: g = gibbsite, h = hematite, k = kaolinite, a = anatase and r = rutile.

XRD phase analysis program (Taylor and Clapp 1992). SIROQUANT uses the cubic (Fd3m) structure determined by Shirasuka et al. (1976) when calculating an XRD pattern for eta-alumina. Refinement of the unit cell parameter from a starting value of a = 7.906 Å was undertaken during the analysis.

The same powder that was used for XRD, was ultrasonically dispersed in ethanol and then pipetted onto a holey carbon-coated grid. TEM was performed on the sample using a JEOL 200CX transmission electron microscope, operating at 200 kV. Selected-area electron diffraction (SAED) patterns of bauxite particles were obtained at a camera length of 74 cm. An SAED pattern displaying a series of diffraction rings was indexed and compared to XRD and calculated d-spacing values.

Analytical TEM (AEM) was undertaken using a nano-probe with a beam diameter of 10 nm in conjunction with energy dispersive X-ray analysis (EDXA) on a Philips 430EM transmission electron-microscope, operating at 300kV.

An infra-red (IR) spectrum of the PDM was obtained using a Perkin Elmer 1800 FTIR spectrophotometer.

RESULTS

The XRD pattern (Figure 1) displays relatively sharp diffraction maxima associated with well-crystallized hematite, gibbsite, anatase, rutile, kaolinite and quartz while broad diffraction maxima are attributed to PDM.

The procedure for obtaining a differential XRD pattern was reasonably effective in removing the well defined peaks associated with gibbsite, hematite and other well-crystallized phases, even though some residual peaks are still evident. The differential XRD pattern displays a series of broad diffraction maxima, similar in intensity and breadth to Weipa akdalaite, but the diffraction lines do not coincide with those of Weipa akdalaite (Figure 2). The broad peaks have maxima that match well with those of η-Al_2O_3 (Stumpf et al. 1950) (Table 1). The 2.0 Å peak has a width (at half maximum) of 1.31 °2θ, which gives a mean crystallite

https://doi.org/10.1346/CCMN.1996.0440508 Published online by Cambridge University Press

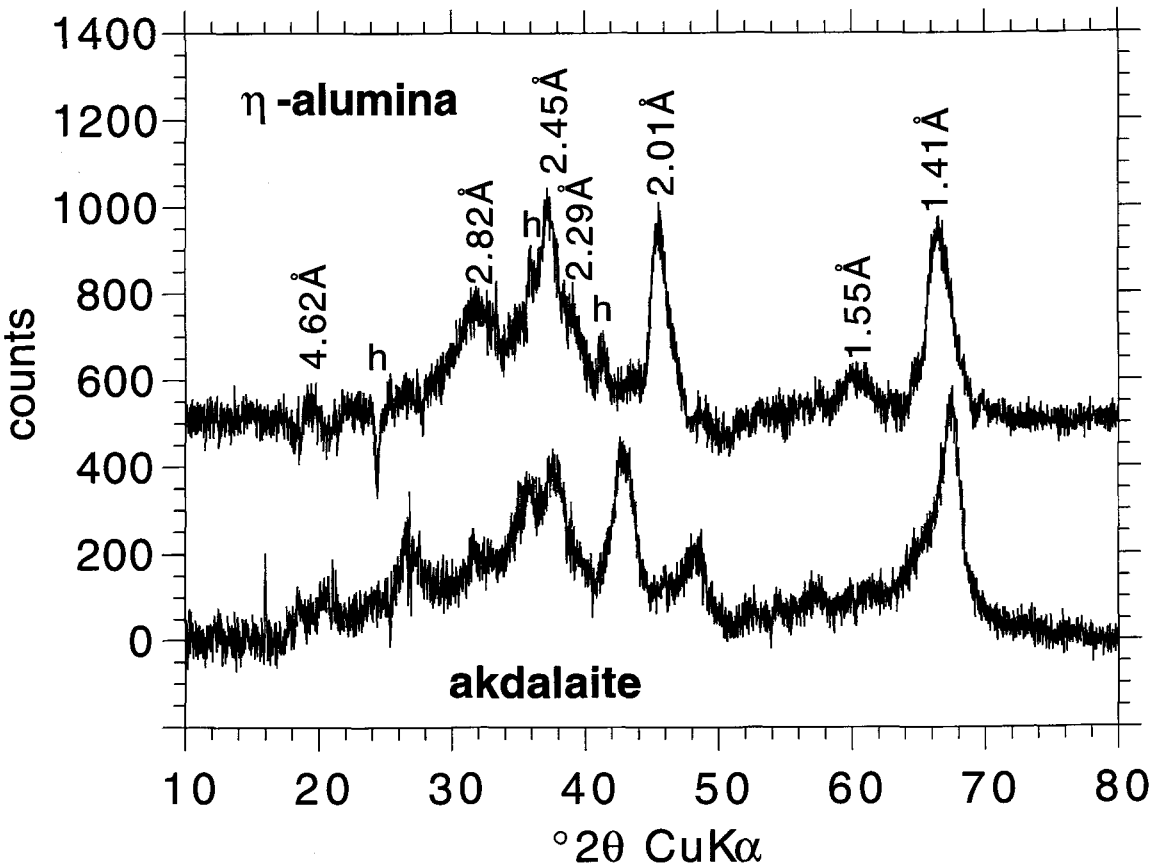

Figure 2. A differential XRD pattern of Andoom η-Al_2O_3 compared with Weipa akdalaite. Under- and over-calculated hematite peaks (h) are labeled.

size of 9 nm when using the Scherrer equation. Quantitative XRD using SIROQUANT indicates that the core of the analyzed pisolith contains greater than 70 wt.% η-Al_2O_3 (Table 2 and Figure 3). Unit cell refinement of Andoom η-Al_2O_3, on the basis of a cubic cell, gives a lattice parameter of a = 7.98 Å.

Extremely fine crystals of approximately 10 nm in width are evident in the TEM image (Figure 4). Those crystals that have lattice fringes of 2.3 and 2.4 Å are associated with η-Al_2O_3. The crystallite size of η-Al_2O_3 determined from the TEM image is close to that calculated using the Scherrer equation (≈9 nm) and is slightly larger than that of Weipa akdalaite (≈6 nm). The d-spacing values obtained from the SAED pattern (Figure 5) coincide well with the XRD pattern of the poorly-diffracting material, indicating that the finely

Table 1. Comparison between the d-spacing values of the PDM determined by electron diffraction, differential XRD and those calculated by Stumpf et al. (1950).

PDM electron diffraction		PDM differential XRD		η-alumina (Stumpf et al. 1950)		
I/I_1†	d Å	I/I_1†	d Å	I/I_1	d Å	hkl
		10	4.62	40	4.6	111
20	2.79	30	2.82	20	2.8	220
80	2.40	80	2.45	60	2.40	311
20	2.28	20	2.29	30	2.27	222
90	1.96	90	2.01	80	1.97	400
20	1.52	20	1.55	20	1.52	333
100	1.39	100	1.41	100	1.40	440
10	1.19			10	1.21	533
20	1.13			20	1.14	444
10	0.98			10	1.03	553
10	0.88					
10	0.80					

† Intensities by visual estimation.

Table 2. quantitative XRD analysis of the PDM-rich material using SIROQUANT.

Phase	Wt%	Error %
eta-alumina	71.6	0.26
Al-hematite	16.7	0.18
gibbsite	8.6	0.18
kaolinite	0.7	0.11
rutile	1.6	0.07
quartz	0.3	0.04
anatase	0.5	0.05

https://doi.org/10.1346/CCMN.1996.0440508 Published online by Cambridge University Press

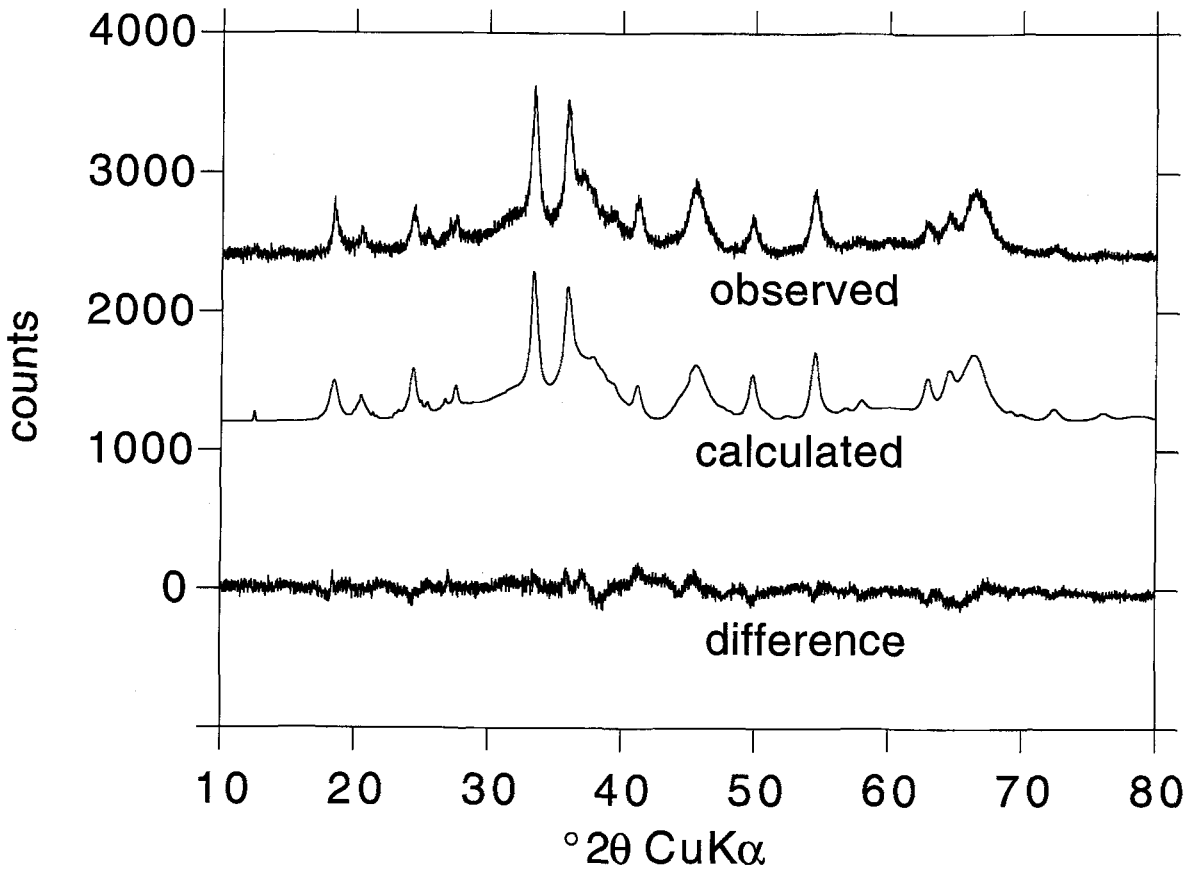

Figure 3. Rietveld-type quantitative-XRD analysis of the bauxite sample containing approximately 70 wt.% η-Al_2O_3.

crystalline material observed using TEM is the same material identified in the XRD pattern.

AEM of randomly selected crystals in the PDM-rich sample revealed the presence of 2 mineral phases: 1) an aluminium-bearing ferruginous phase; and 2) an almost pure aluminous phase (Table 3). The most ferruginous particle analyzed contained 22 *M*% Al while the most aluminous one had <2 *M*% Fe.

A transmittance infra-red spectrum of the material containing approximately 70 wt.% PDM, shows a broad absorption band at 3450 cm^{-1} due to O-H stretching and at 1630 cm^{-1} associated with O-H bending vibrations (Figure 6).

DISCUSSION

The XRD patterns of synthetic eta- and gamma-alumina are known to very similar (Spitler and Pollack 1981; Zhou and Snyder 1991). However, there are small but measurable differences that can be used to distinguish between the 2 phases. The most useful discriminator is at approximately 1.98 Å, where η-Al_2O_3 has 1 strong line while γ-Al_2O_3 has a doublet consisting of a strong line at 1.98 Å and a strong shoulder at 1.95 Å. We conclude that PDM from Andoom is composed of η-Al_2O_3 rather than γ-Al_2O_3 because although slightly asymmetric, the 1.98 Å peak appears single. Though as yet undiscovered, the existence of γ-Al_2O_3 in bauxites is highly probable.

The aluminium-bearing ferruginous phase analyzed by AEM is ascribed to Al-hematite while the almost pure aluminous phase is attributed to η-Al_2O_3. AEM indicates the Al-hematite may contain up to 22 *M*% Al. Unit cell refinement of the hematite gave cell parameters of a, b = 5.0118 Å and c = 13.7120 Å, indicating an Al substitution of between 20 and 23 *M*% (Schwertmann 1988a; Stanjek 1991), assuming a formation temperature of between 25 and 40 °C. However, Schwertmann (1988b) reported that no soil hematites have been found that contain greater than 18 *M*% Al. In fact, Al-substitution in hematite may be limited to ⅙ of the possible octahedral positions, that is, 17 *M*% Al (Schwertmann 1988a). Although every effort was made to ensure that the analyses were obtained from individual crystals, it is possible that characteristic Al X-rays from an adjacent alumina grain may have led to an apparently high Al content for the hematite. Due to this inconclusiveness, a value of 18 *M*% Al was chosen for hematite's site occupancy. A

https://doi.org/10.1346/CCMN.1996.0440508 Published online by Cambridge University Press

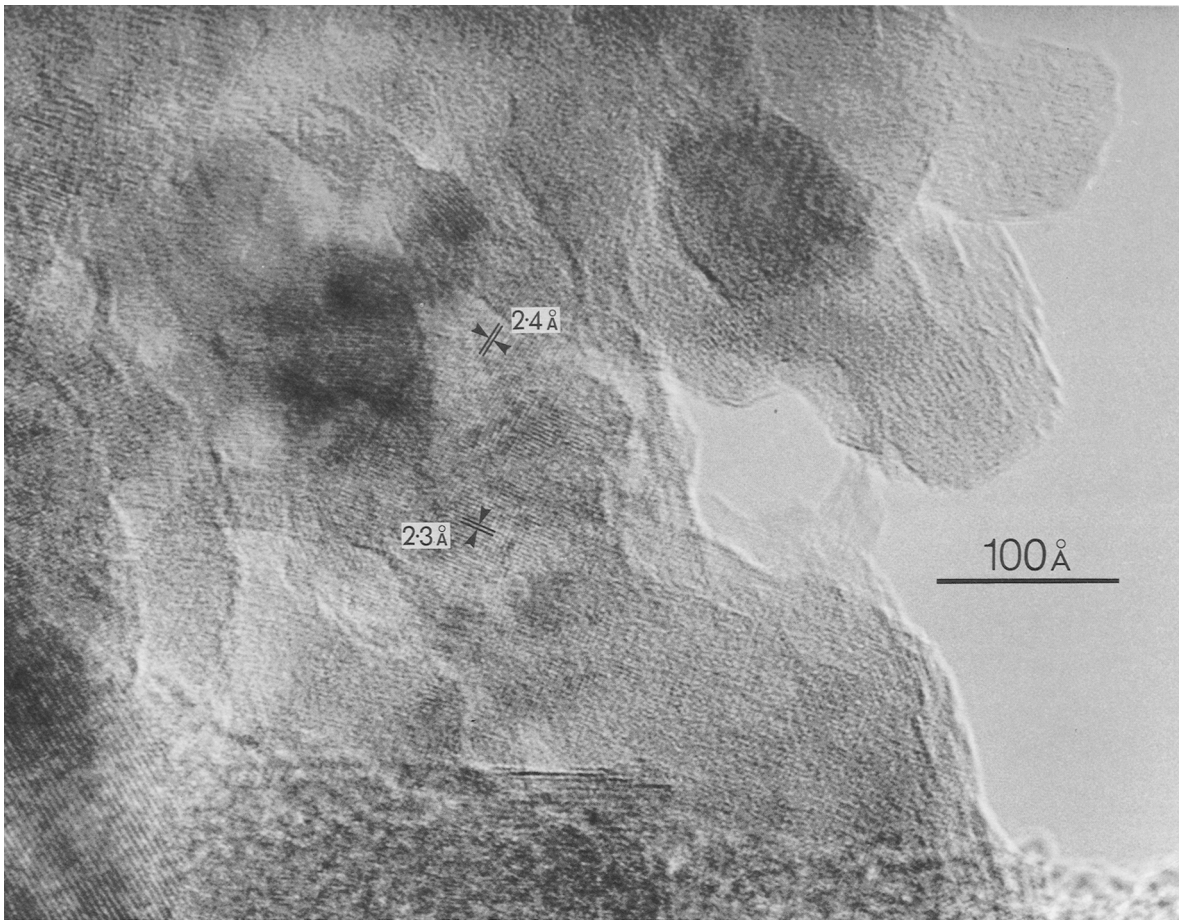

Figure 4. A TEM of one particular area in the poorly diffracting material. The crystal size of the PDM is approximately 10 nm. Lattice fringes of 2.3 and 2.4 ° indicate η-Al_2O_3.

close match between the observed and calculated XRD patterns was obtained using this value. Quantification of the bauxite's mineralogy was also performed using the same site occupancy.

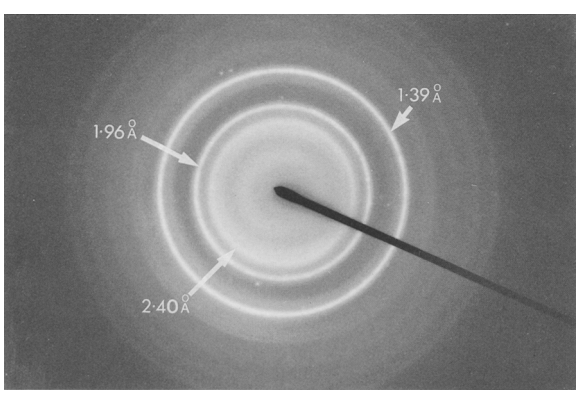

Figure 5. An SAED pattern of Andoom η-Al_2O_3.

The H_2O contained within the crystal lattices of gibbsite is 34.6 wt.%, boehmite is 15.0 wt.%, and akdalaite is 4.4 wt.%. The theoretical crystalline structure of η-Al_2O_3 contains no chemically-bonded water. Both akdalaite and η-Al_2O_3 contain appreciable amounts of strongly adsorbed H_2O as evidenced by their transmittance IR spectra, but the actual amount is not determinable from the spectra alone. The reason for the large amount of adsorbed water is presumed to be mainly to their large surface areas. For example, the surface area of 1 g of η-Al_2O_3 (ρ = 3.63 g/cm^3) assuming it consists of an aggregate of cubic crystals, is approximately 2200 m^2/g.

The discovery of akdalaite and η-Al_2O_3 in the bauxites of Weipa and Andoom has greatly expanded our knowledge and understanding of bauxite mineralogy and the role H_2O activity may play in the evolution of bauxitic pisoliths. The majority of concentrically-banded bauxitic pisoliths and those with PDM-rich cores evolve in a similar manner to that proposed by Tardy and Nahon (1985), except that ak-

https://doi.org/10.1346/CCMN.1996.0440508 Published online by Cambridge University Press

Table 3. Nano-probe analyses of individual crystals in the PDM-rich bauxite sample. The analytical total has been recalculated to 100%.

	eta-alumina				eta-alumina + Al-hematite					Al-hematite	
	1	2	3	4	5	6	7	8	9	10	11
wt%											
Al_2O_3	96.4	95.7	95.5	95.1	91.1	88.5	36.3	29.8	23.0	18.6	15.4
SiO_2	0.6	0.8	1.4	0.8	0.0	0.9	0.0	0.6	0.3	0.0	0.0
TiO_2	0.7	1.1	0.9	1.0	0.1	0.0	1.3	2.6	2.2	2.4	2.4
Fe_2O_3	2.3	2.4	2.2	3.1	8.8	10.6	62.5	67.0	74.4	78.9	82.3
cation %											
Al	97.6	97.0	96.8	96.6	94.1	92.1	47.2	39.9	31.9	26.4	22.2
Si	0.5	0.7	1.2	0.7	0.0	0.8	0.0	0.7	0.4	0.0	0.0
Ti	0.4	0.7	0.6	0.6	0.1	0.0	1.0	2.2	2.0	2.2	2.2
Fe	1.5	1.5	1.4	2.0	5.8	7.1	51.8	57.3	65.8	71.4	75.7

dalaite or η-Al_2O_3 may epigenetically replace kaolinite during nodule development as well as Al-hematite. Troland and Tardy (1987) showed that at 25 °C the chemical activity of water was a major factor in determining the degree of hydration in bauxite minerals. If the kaolinite grains within the developing nodule are very small, then the intercrystalline voids are correspondingly so. As the weathering profile dries out, water is retained in progressively smaller pores with correspondingly lower H_2O activities (Tardy and Nahon 1985). The activity of H_2O within pores may be so low that anhydrous phases such as Al-hematite and η-Al_2O_3 may form. Where pore sizes are a little larger and a slightly higher H_2O activity prevails, boehmite becomes the dominant Al-rich mineral. In the largest voids gibbsite normally crystallizes, as the H_2O activity is usually too high for the less hydrated phases to form.

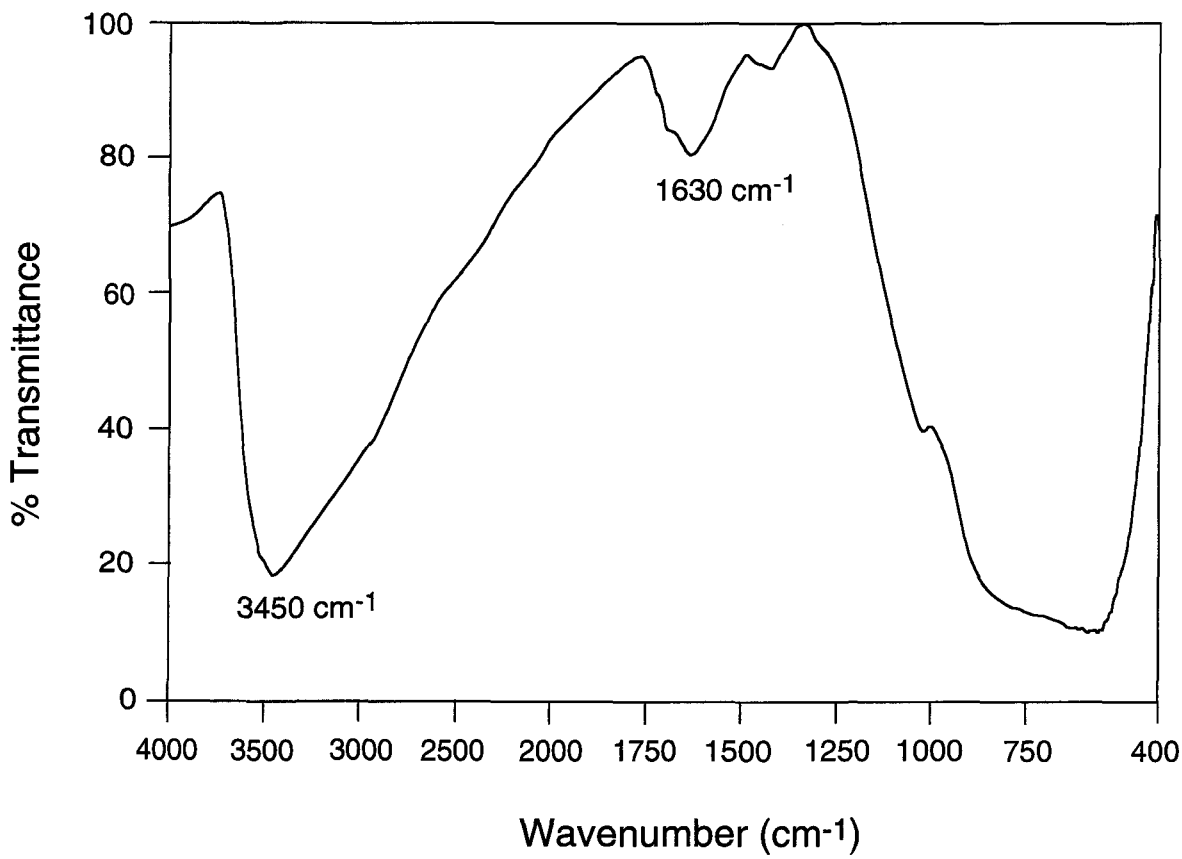

Figure 6. A transmittance infra-red spectrum of bauxitic material containing approximately 70 wt.% η-Al_2O_3.

https://doi.org/10.1346/CCMN.1996.0440508 Published online by Cambridge University Press

ACKNOWLEDGMENTS

This work was supported by a research grant from COMALCO Aluminium Limited, for which we are most appreciative. SEM was performed using the facilities of the EM unit at the Research School of Biological Sciences, ANU. D. Bogsànyi of the Research School of Chemistry, ANU acquired the infrared spectrum. Analytical TEM using the nano-probe was undertaken at the Research School of Earth Sciences, ANU.

REFERENCES

Brown JF, Clark D, Elliott WW. 1953. The thermal decomposition of the alumina trihydrate, gibbsite. J Chem Soc 13:84–88.

Lippens BC, de Boer JH. 1964. Study of phase transformations during calcination of aluminium hydroxides by selected-area electron diffraction. Acta Crystall 17:1312–1321.

Schwertmann U. 1988a. Some properties of soil and synthetic iron oxides. In: Stucki JW, Goodman BA, Schwertmann U, editors. Iron in soils and clay minerals. Dordrecht, Holland: D. Reidel Publishing Company. p 203–250.

Schwertmann U. 1988b. Occurrence and formation of iron oxides in various pedoenvironments. In: Stucki JW, Goodman BA, Schwertmann U, editors. Iron in soils and clay minerals. Dordrecht, Holland: D. Reidel Publishing Company. p 267–308.

Shirasuka K, Yanagida H, Yamaguchi G. 1976. The preparation of η-alumina and its structure. Yogyo Kyokai Shi 84:610–613.

Singh B, Gilkes RJ. 1995. The natural occurrence of χ-alumina in lateritic pisolites. Clay Miner 30:39–44.

Spitler CA, Pollack SS. 1981. On the X-ray diffraction patterns of η- and γ-alumina. J Catal 69:241.

Stanjek H. 1991. Aluminium- und Hydroxylsubstitution in synthetischen und natürlichen Hämatiten. Buch am Erlbach, Germany: Verlag Marie L. Leidorf. 194 p.

Stumpf HC, Russell AS, Newsome JW, and Tucker CM. 1950. Thermal transformations of aluminas and alumina hydrates. Ind Eng Chem 42:1398–1403.

Tardy Y, Nahon D. 1985. Geochemistry of laterites, stability of Al-goethite, Al-hematite, and Fe^{3+}-kaolinite in bauxites and ferricretes: an approach to the mechanism of concretion formation. Am J Sci 285:865–903.

Taylor JC, Clapp RA. 1992. New features and advanced applications of SIROQUANT: A personal computer XRD full profile quantitative analysis software package. Adv X-ray Anal 35:49–55.

Tilley DB, Eggleton RA. 1994. Tohdite ($5Al_2O_3 \cdot H_2O$) in bauxites from northern Australia. Clays Clay Miner 42: 485–488.

Troland F, Tardy Y. 1987. The stabilities of gibbsite, boehmite, amorphous goethites and aluminous hematites in bauxites, ferricretes and laterites as a function of water activity, temperature and particle size. Geochim Cosmochim Acta 51:945–957.

Zhou R, Snyder RL. 1991. Structures and transformation mechanisms of the η, γ and θ transition aluminas. Acta Crystall B47:617–630.

(Received 29 June 1995; accepted 31 December 1995; Ms. 2665)